

# Future Atmospheric Rivers in Antarctica : intensity and impacts

Léonard Barthélemy<sup>1</sup>, Francis Codron<sup>2</sup>, Vincent Favier<sup>3</sup>, and Jonathan Wille<sup>4</sup>

<sup>1</sup>French National Centre for Scientific Research

<sup>2</sup>LOCEAN, Sorbonne Université/CNRS/IRD/MNHN

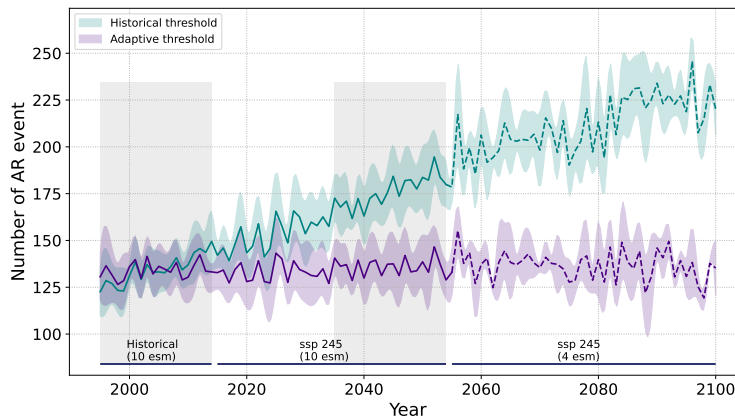
<sup>3</sup>Université Grenoble Alpes - CNRS

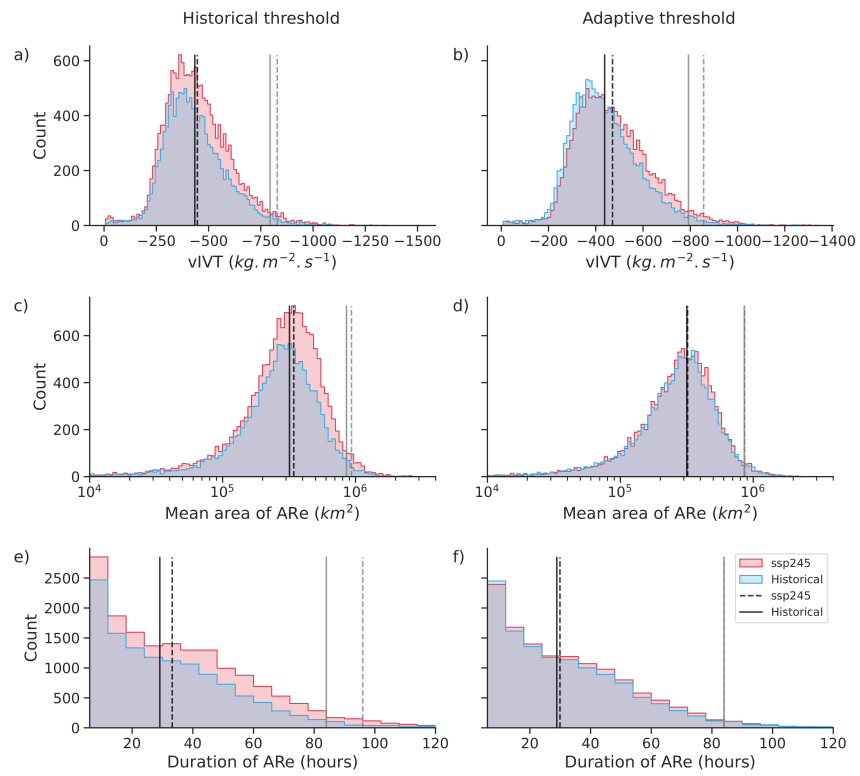
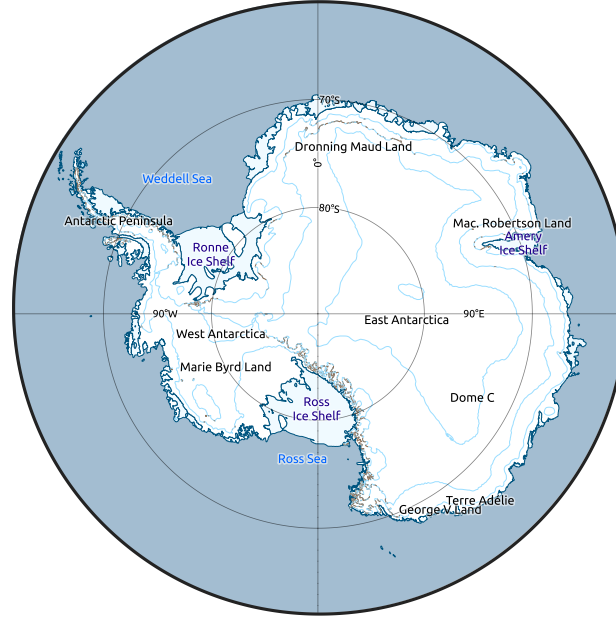
<sup>4</sup>ETH Zurich

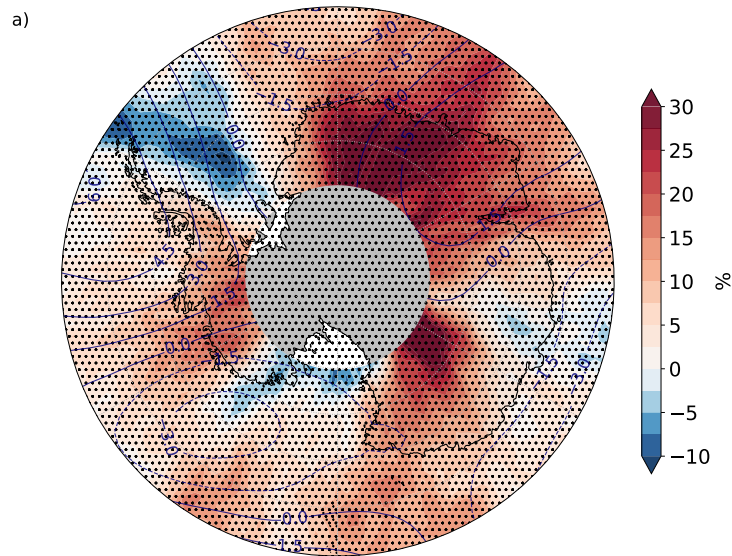
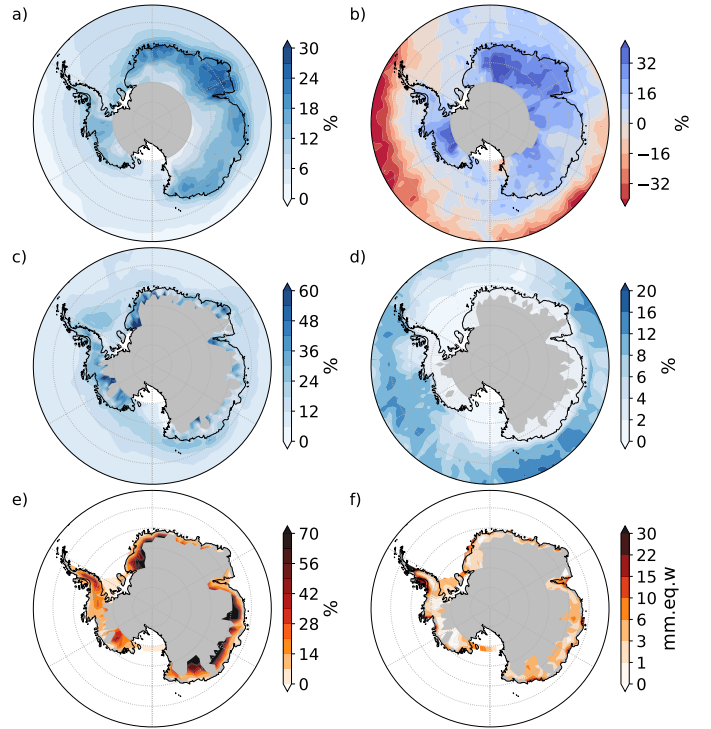
April 23, 2024

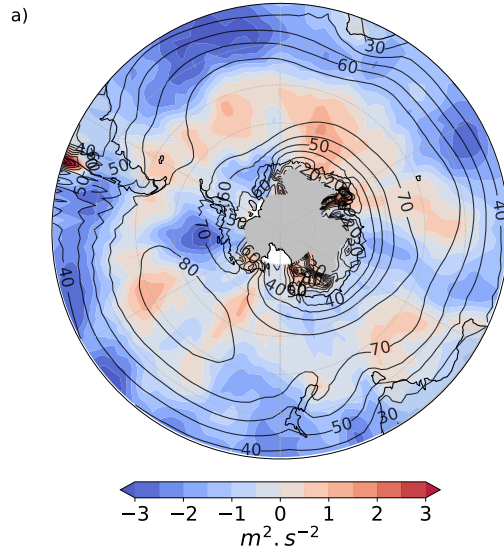
## Abstract

Atmospheric rivers (ARs) are extreme hydrological events that have strong impacts on the Antarctic surface mass balance (SMB), through both snow accumulation and surface melt due to heating and rain. To estimate their impacts on future SMB, we study Antarctic ARs in an ensemble of 21st century simulations. While the number of detected ARs increases continuously when using a constant detection threshold based on historical moisture fluxes, it remains stable with an adaptive threshold evolving with the rising background moisture. However, ARs penetrate further into Antarctica following a wave number 3 pattern. In addition, the intensity of Antarctic ARs, measured by moisture fluxes, is simulated to increase following the Clausius-Clapeyron relation. The opposing SMB impacts become larger, with both increasing snowfall, and coastal surface melt and rainfall. Yet, their overall influence on the SMB is dominated by increased snow accumulation.









# Future Atmospheric Rivers in Antarctica : intensity and impacts

L.Barthélemy<sup>1</sup>, F.Codron<sup>1</sup>, J.Wille<sup>2</sup>, V.Favier<sup>3</sup>

<sup>1</sup>Laboratoire d'Océanographie et du Climat, LOCEAN-IPSL, Sorbonne Université, CNRS, IRD, MNHN,  
Paris, France

<sup>2</sup>Institute for Atmospheric and Climate Science, ETH Zurich, Zurich, Switzerland

<sup>3</sup>Institut des Géosciences de l'Environnement, CNRS/UGA, Saint Martin d'Heres, France

## Key Points:

- The evolution of future Antarctic atmospheric river frequency strongly depends on detection threshold adjustments to increasing moisture.
- Future Antarctic atmospheric river frequency overall remains stable, but with regional increases due to circulation changes.
- Snowfall dominates future surface mass balance change from Atmospheric Rivers, despite increasing rainfall and melt.

## Abstract

Atmospheric rivers (ARs) are extreme hydrological events that have strong impacts on the Antarctic surface mass balance (SMB), through both snow accumulation and surface melt due to heating and rain. To estimate their impacts on future SMB, we study Antarctic ARs in an ensemble of 21st century simulations. While the number of detected ARs increases continuously when using a constant detection threshold based on historical moisture fluxes, it remains stable with an adaptive threshold evolving with the rising background moisture. However, ARs penetrate further into Antarctica following a wave number 3 pattern. In addition, the intensity of Antarctic ARs, measured by moisture fluxes, is simulated to increase following the Clausius-Clapeyron relation. The opposing SMB impacts become larger, with both increasing snowfall, and coastal surface melt and rainfall. Yet, their overall influence on the SMB is dominated by increased snow accumulation.

## Plain Language Summary

The Antarctic is the largest freshwater store on Earth, and could make a major contribution to sea-level rise in the future. Atmospheric rivers are extreme hydrological events that have significant impacts on surface mass balance. Using a modeling study, we find out that the AR frequency over Antarctica increases slightly in a future climate, but their impacts are much larger, especially the associated snowfall that increases faster than the mean.

## 1 Introduction

The Antarctic ice sheet represents the world's largest freshwater reserve, and could contribute to a sea level rise of 58.3m (Fretwell et al., 2013) if all the ice melted. The Antarctic mass balance is therefore a key player in future sea-level rise. Although the contribution of loss by calving is critical, the surface mass balance (SMB) also plays a major role in regional variations, particularly in East Antarctica (Wessem et al., 2014). Future variations in the snowfall are expected to follow the Clausius-Clapeyron relation, but remain largely uncertain. Currently, the SMB is driven mainly by variations in heavy precipitation events (Turner et al., 2019), in particular by Atmospheric Rivers (ARs) (Wille et al., 2021).

ARs are atmospheric water vapor transport events that are rare but contribute significantly to the exchanges between mid and high latitudes (around 90% of meridional water vapor transport is linked to ARs, (Nash et al., 2018)). Over Antarctica, they dominate the variability of snowfall (Gorodetskaya et al., 2014), but can also lead to rainfall and warm extremes through advection of warm air and increased downward long-wave radiation from liquid-laden clouds (Wille et al., 2019), which will contribute negatively to the SMB.

On a global scale, an increase in AR frequency is projected and in fact already observed (Shields et al., 2023). However, AR detection algorithms use thresholds based on moisture fluxes that are sensitive to the rise in mean moisture content in a warmer climate through the Clausius-Clapeyron relation. Attempts to separate the drivers of projected AR changes have shown that the predicted increase is dominated by this thermodynamic effect (Baek & Lora, 2021), while changes in atmospheric dynamics rather lead to a redistribution of ARs with little change in frequency.

The systematic study of future AR behaviour in the Antarctic region has been largely ignored so far, as polar ARs are rarer and require polar-specialised detection algorithms (Wille et al., 2019; Shields et al., 2023). While relatively recent trends in Antarctic AR have been documented for the recent period in Antarctica (Payne et al., 2020) no stud-

ies have yet focused on future Antarctic ARs. Here, we use the IPSL-CM6 model to study the evolution of ARs in Antarctica and their impacts on precipitation and melt. We first construct an AR catalog using a polar-specialised algorithm with an adaptive threshold to remove the impact of increasing background moisture and isolate the role of atmospheric dynamics. We then look at the future evolution of AR occurrence, the intensity of the associated water vapor transport, and quantify their impacts on the different components of the SMB.

## 2 Data and Methods

### 2.1 IPSL-CM6 coupled GCM

We use output from ensembles of CMIP6 simulations with the IPSL-CM6 model (Boucher et al., 2018). The IPSL model resolution is  $2.5^\circ$  longitude by  $1.267^\circ$  latitude, and its physics have been adjusted and validated for the Antarctic climate (Vignon et al., 2018). Integrated water vapor (IWV) content and fluxes were reconstructed using 6-hourly outputs on model levels. Concerning AR impacts, we use daily precipitation, 2-m temperature and surface fluxes. 10 members of this model with the required data were available until the year 2055, but only 4 afterwards. Therefore when comparing the present and future ARs, we will use two 20-years periods; historical (1995-2015) and future (2035-2055) using the ssp245 scenario.

### 2.2 AR detection and event clustering

We use the polar-adapted AR detection algorithm described in Wille et al. (2021), based on the meridional component of the water vapor transport integral (vIVT) :

$$vIVT = -\frac{1}{g} \int_{1000hPa}^{0hPa} qv dp \quad (1)$$

where  $q$  is the specific humidity,  $v$  the meridional wind velocity, and  $p$  the atmospheric pressure. At each time step, the algorithm detects continuous sets of grid points between  $38^\circ S$  and  $80^\circ S$  where the value of vIVT is greater or equal than a detection threshold, with at least  $20^\circ$  extent in latitude.

The detection threshold is based on the 98th percentile of monthly vIVT in the historical climate. However, in the context of climate change, the progressive increase of water vapor content leads to a shift of the vIVT distribution and a spurious increase of detected events (i.e. events that are not extremes in their background climate). We thus use an adaptive threshold that takes into account the evolution of the background water vapor content, measured by IWV:

$$Adaptive\ threshold = \frac{IWV_{yearly\ mean}^{60S-38S}}{IWV_{historical\ mean}^{60S-38S}} \quad (2)$$

With  $IWV_{yearly\ mean}^{60S-38S}$  as the annual average between  $60^\circ S$  and  $38^\circ S$  and  $IWV_{historical\ mean}^{60S-38S}$  as the historical climatic average over the same area. The Southern Ocean region was chosen because it is the transit corridor for ARs reaching Antarctica. These raw annual values of the adaptive threshold coefficient are smoothed by a linear trend to remove interannual variability, then multiplied by the 98<sup>th</sup> percentile of historical vIVT to obtain the adaptive detection threshold.

The detection algorithm identifies the area occupied by ARs at each time step. We then constructed a catalog of AR events by separating individual ARs at a given time using a clustering method, then follow these ARs over time with a criteria based cluster motion. Each AR events is characterized by its times of occurrence and occupied grid

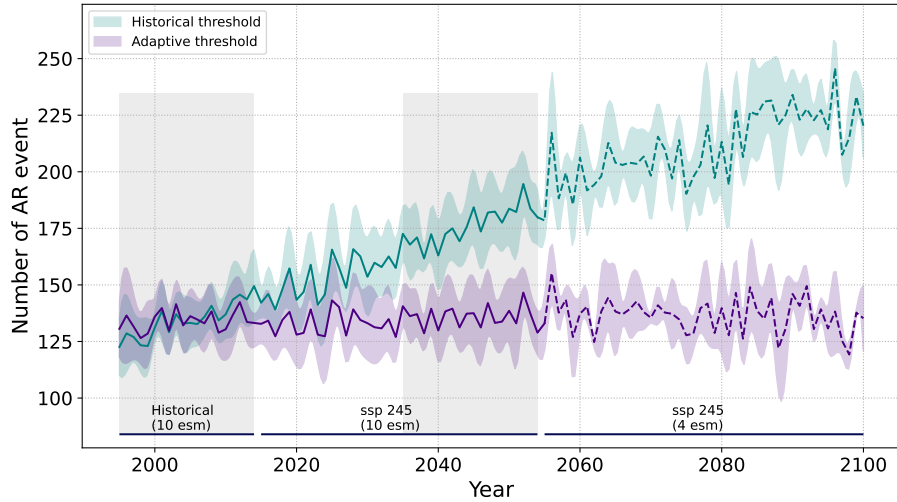


**Figure 1.** Time series of the yearly number of AR events. Green line represents the historical threshold based on the historical (1995-2015) period and the indigo line represents the adaptive threshold normalized by the Southern Ocean IWV (38°S to 60°S). 10 members (esm) were used until 2055, 4 members (dashed line) afterwards. The uncertainty envelope (shading) is given by:  $\pm\sigma \times \sqrt{\frac{n}{n-1}}$ . The grey shaded boxes outline the periods used to determine future AR frequency.

106 points, allowing to compute the corresponding vIVT value, maximum temperature and  
 107 precipitation amount, and to define AR events duration or intensity, as used for exam-  
 108 ple by Ralph et al. (2019) to construct a scale for mid-latitude ARs.

### 109 2.3 Threshold Influence

110 AR events were computed using both the constant historical threshold and the adap-  
 111 tive threshold (figure 1). With the fixed historical threshold, the average yearly num-  
 112 ber of detected AR events increases steadily until it nearly doubles by 2100 (83.5% in-  
 113 crease). Note that an upward trend is already seen during the historical period, show-  
 114 ing that observed AR frequency trends should be interpreted cautiously.

115 With the adaptive threshold however, no significant trend is observed and the num-  
 116 ber of AR events fluctuates around 135 per year. The adaptive threshold therefore com-  
 117 pensates rising background moisture effect and explains most of the increasing AR trend  
 118 seen when using a historical threshold. On interannual timescales, the two series are cor-  
 119 related at 75%.

## 120 3 Results

### 121 3.1 Atmospheric Rivers Frequency

122 Antarctic ARs, defined using a 98% vIVT threshold, are very rare events, as shown  
 123 by Wille et al. (2021). For the historical period, the AR frequency, defined as the per-  
 124 centage of all time steps when an AR is detected at a given point, is highest across all  
 125 longitudes over the Southern Ocean (0.72% at 58°S) and decreases gradually towards Antarc-  
 126 tica (0.65% at 70°S). These values are similar, albeit slightly smaller, to the ones found  
 127 by Wille et al. (2021) using reanalysis products.

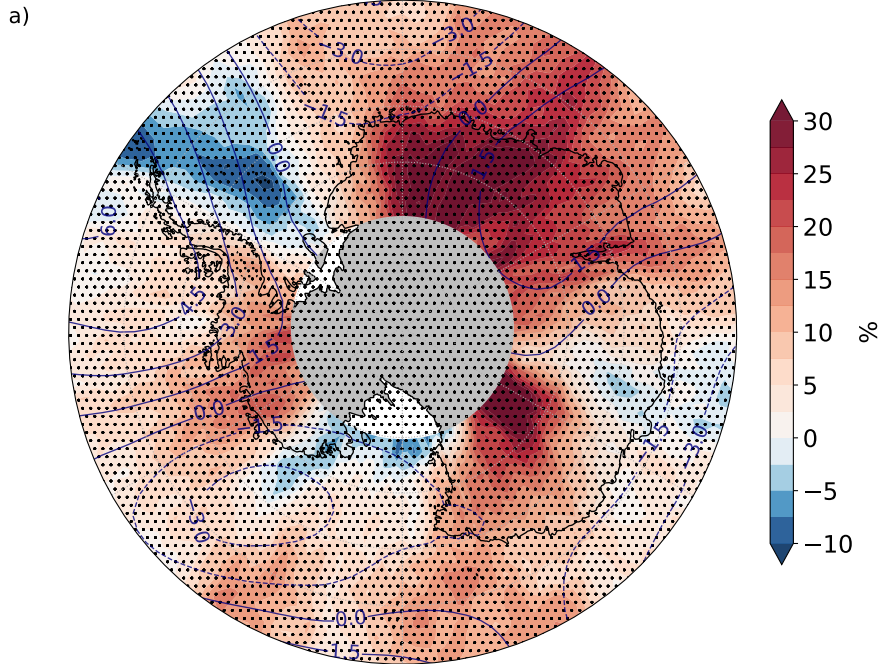


**Figure 2.** Relative difference in AR detection frequency between the future and historical periods using the adaptive threshold (colors). Dots mark 95% confidence (assuming that the number of detected ARs follows a Poisson distribution). Lines: 500hPa geopotential difference between the two periods, with the zonal mean removed.

128 This structure is similar for the 2035-2055 period, with a small but significant in-  
 129 crease in AR frequency around Antarctica, even with the adaptive threshold. The re-  
 130 lative differences between the two periods (Figure 2) shows a 5% increase for the Antarc-  
 131 tic area (table 1). This is consistent with the dynamically-driven increase of AR frequency  
 132 found in other studies caused by the future poleward shift of the jet and storm tracks  
 133 (Zhang et al., 2024).

134 In addition, a wave-number 3 pattern is clearly apparent, with large AR frequency  
 135 increases in the Dronning Maud Land area, (+33.6% relative increase), the Dome C re-  
 136 gion (+39.9%), and Marie Byrd Land (+21.5%). Elsewhere, there is little increase or in-  
 137 significant decrease. This wave number 3 pattern is consistent with the future changes  
 138 in mean circulation, as shown on figure 2 by the 500-hPa geopotential heights difference.  
 139 The increases in AR frequency roughly coincide with regions of increased poleward merid-  
 140 ional wind. This could be caused by either by a direct local increase in the mean pole-  
 141 ward moisture transport, or indirectly by a change in the storm trajectories and inten-  
 142 sities (fig. S1).

### 143 3.2 Intensity of AR events

144 Concerning AR events, figure 3 shows the distribution of three key characteristics  
 145 (intensity, area, and duration) for the two periods considered using both historical and  
 146 variable adaptive thresholds. Only ARs that reached the Antarctic continent at some  
 147 time during their life cycle are considered. On average, 61 such events per year were de-  
 148 tected over the historical period. This increases to 64 events for the future period with  
 149 an adaptive threshold (5% increase, same as the AR detection frequency), and to 80 events  
 150 with a historical threshold (30% increase).

151 This increase on the number of AR events with a historical threshold is reflected  
 152 in the AR characteristic distributions (figure 3), with all AR metrics showing increases  
 153 in the future period . This includes increases in the mean event area and duration, prob-  
 154 ably due again to a detection threshold that is more easily crossed in the future. Con-  
 155 versely, there is almost no change in mean event area when using the adaptive thresh-  
 156 old, and only a small increase in mean event duration (about 1 hour, with a mean du-  
 157 ration of 30 hours).

158 The changes in AR event intensity also show a different behavior between the two  
 159 methods. With the historical threshold, the event frequency for all intensities increases,  
 160 but the mean intensity does not change much. By contrast, with an adaptive threshold  
 161 there is little change in the total number of events, but importantly a shift of the dis-  
 162 tribution towards more intense events. The mean event intensity increases by 7.5%, which  
 163 is close to the IWV increase observed in the Southern Ocean used in the adaptive thresh-  
 164 old definition (+7.7%). The frequency of extreme ARs increases even more, with +108%  
 165 of events exceeding  $900 \text{ kg.m}^{-2}.\text{s}^{-1}$  in the future.

### 166 3.3 Impact on SMB

167 The SMB of the Antarctic ice sheet is the balance of the accumulation and erosion  
 168 terms of the snow surface.

169 The ARs impact several components of the SMB. The advection of relatively warm  
 170 and moist air over the continent leads to high accumulation rates (snowfall), but poten-  
 171 tially also surface melt because of high sensible fluxes and especially downwards long-  
 172 wave radiation (Bozkurt et al., 2018; Neff et al., 2014).

173 ARs can also lead to rainfall events, which have an ambiguous impact on the SMB  
 174 : liquid precipitation is part of the accumulation term, but can also lead to more melt-  
 175 ing through the associated heat fluxes and its impact on snow albedo (Vignon et al., 2021).

176 Here we focus on the evolution of AR impacts on the SMB. The quantities (melt  
 177 or precipitation) are considered AR-related if they occur when an AR is detected at a  
 178 given grid point at a particular time step, and up to 24 hours afterwards (to allow for  
 179 a delay between the water vapor advection and its impacts). Table 1 summarizes the key  
 180 SMB changes (integrated and averaged) over the Antarctic continent between the present  
 181 and future periods, both for total SMB changes and AR-related SMB changes.

#### 182 3.3.1 Precipitation

183 We distinguish between solid and liquid precipitation because of their differing SMB  
 184 impacts. Snowfall accounts for the largest share of total precipitation in Antarctica (99.5%  
 185 of precipitation over the historical period is snowfall, see table 1), while rainfall accounts  
 186 for a negligible volume but can have large impacts locally.

187 Overall, there was a +9.3% increase in total precipitation volume between the present  
 188 and future periods. This is somewhat larger than the increase in water vapor over the  
 189 Southern Ocean (+8% increase in IWV, presumably following the Clausius-Clapeyron  
 190 relation), but less than the IWV increase over the continent (+12.7%). This increase is  
 191 dominated by snowfall following the climatology, but the rainfall component is increas-  
 192 ing much more rapidly (+98%).

193 AR-related snowfall can contribute locally up to 33% of annual precipitation, mostly  
 194 near coastal regions and in East Antarctica, where the maximum contribution is found  
 195 in Mac Robertson Land near the Amery ice shelf (fig. 4a). The AR contribution is much  
 196 weaker over the ocean, where lots of precipitation falls as rain within storms and because  
 197 the ARs-related snow precipitation comes from the orographic ascent of water vapour

when the ARs arrive on the continent. The global pattern is close to the results of Wille et al. (2021) obtained with Regional Atmospheric Model (MARv3.10.2) forced by ERA5 even if the values of the contributions are slightly higher with the IPSL-CM6 model.

The future change of AR-related snowfall shows a different pattern (fig. 4b). Snowfall increases over the continent, with a maximum of +55% in Dronning Maud Land and follows a wave-number 3 structure similar to the relative increase in AR detection frequency (Fig. 2). Conversely, AR-related snowfall decreases over the Southern Ocean, because of the transition from snow to rain in a warmer climate.

While the rainfall associated with the ARs is low in absolute quantities, it can represent a very high share of total rainfall. The ARs bring liquid precipitation close to the coast but occasionally to the hinterlands slightly inland. Indeed, the contribution of AR-related rainfall is highest in these areas (fig. 4c), with up to 100% in areas such as Coats Land and Marie Byrd Land. Large contributions are also found in the Weddell Sea and on the continental slope in front of George V Land.

The future increase in AR-related rainfall is largest over the Southern Ocean where it replaces snowfall (fig. 4d), but the relative increase over the continent is still very large (+76%, table 1), although smaller than for the total rainfall. A closer comparison over the continent shows that rainfall is not closely related to ARs increases in coastal regions, where the rainfall threshold is reached more easily in the warmer climate regardless of ARs. There is however an increase in AR-related rainfall further inside the continent, where this threshold was never previously crossed.

### 3.3.2 Melt

Surface melt is also an important part of the Antarctic SMB. Even though direct mass loss from surface melt is negligible compared to the mass loss via ice discharge, surface melt still indirectly influences ice discharge through albedo change (Jakobs et al., 2019), firn densification (Datta et al., 2019; Kuipers Munneke et al., 2018) and ice shelf destabilization (Pollard et al., 2015).

The IPSL-CM6 model does not provide direct information on the amount of surface melt or runoff over Antarctica. We therefore estimate it from the surface energy budget:

$$Q = LW \downarrow + SW \downarrow - LW \uparrow - SW \uparrow - H - LE \quad (3)$$

where  $Q$  is the energy balance of the ice sheet surface,  $LW$  and  $SW$  the short- and long-wave radiation ( $\uparrow$  upwards and  $\downarrow$  downwards),  $H$  and  $LE$  the turbulent fluxes of sensible and latent heat. For days when the temperature is above  $-1^\circ\text{C}$  degrees and the energy balance  $Q$  is positive towards the surface, the mass of melted water is calculated as follows:

$$M = \frac{Q_{day} \times 86400}{L} \quad (4)$$

where  $M$  is the mass of melted water ( $\text{kg}\cdot\text{m}^{-2}\cdot\text{day}^{-1}$  or  $\text{mm}\cdot\text{w.e.}\cdot\text{day}^{-1}$ ),  $Q_{day}$  the daily-mean energy balance ( $\text{W}\cdot\text{m}^{-2}$ ), and  $L$  the latent heat of ice melt ( $334\text{kJ}\cdot\text{kg}^{-1}$ ).

As with precipitation, melting is associated with an AR up to one day after its detection. Just like total melt, AR-related melt is concentrated at the edges of the continent, but the share of ARs in the total increases inland, reaching 100% in areas such as the beginning of the Adélie Land plateau and Coats Land (fig. 4e).

The future changes show a significant increase in AR-related melting on the coast and especially on the peninsula (+107mm eq w) and also on some sensitive ice shelves like Ameriy ice shelf (+103% of mm eq w melted) and Filchner ice shelf (+108%), but as for rainfall the greatest relative differences are found on the plateau in areas where melt did never occur in the present climate.

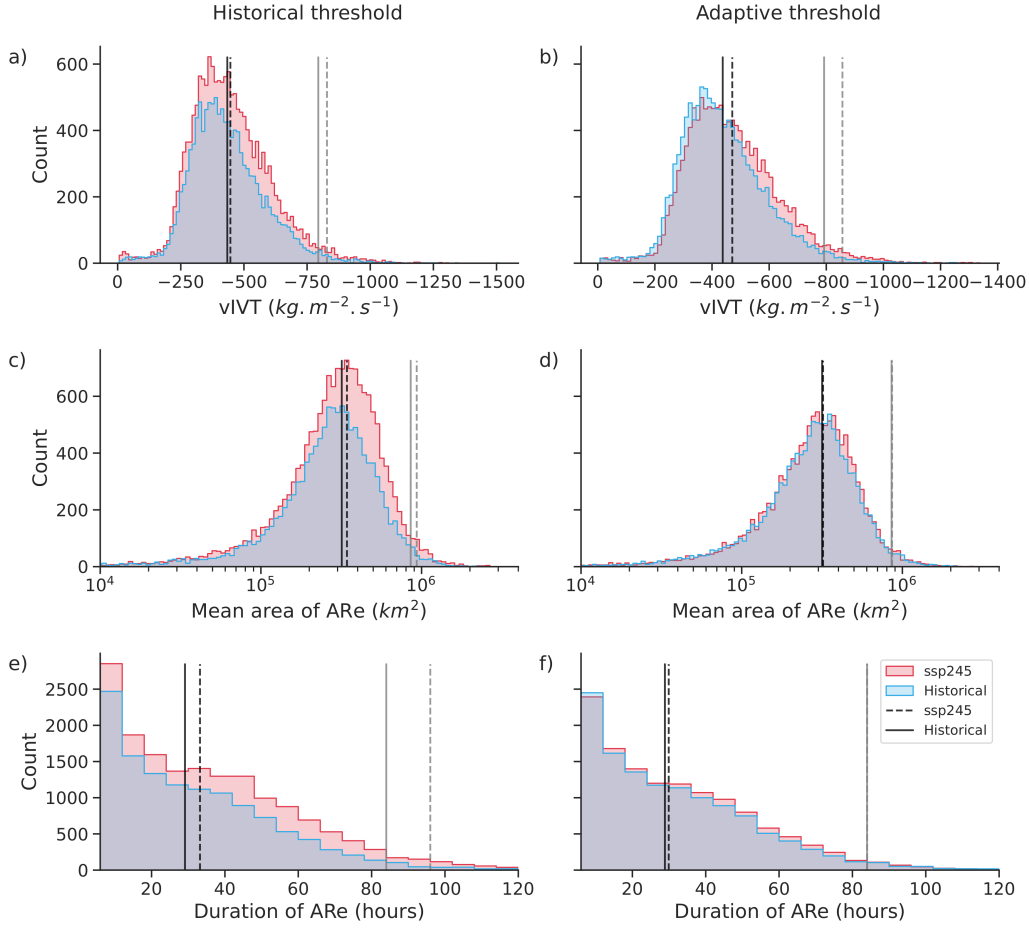


**Figure 3.** Distributions of AR events (ARe) characteristics in the historical (blue shading and solid vertical lines) and future (red shading and dotted vertical lines) periods, for a historical (left) and adaptive (right) threshold. Only AR events reaching Antarctica are used. The vertical lines indicate the mean (black) and 98th percentile (grey) of each distribution. **a,b)**, maximum southward vIVT during the event. **c,d)**, average area of the AR events (in  $km^2$ ). **e,f)**, total duration of AR events in hours.

Variable	Global Antarctica			AR impact		
	Hist	Future	Rel. chg. (%)	Hist	Future	Rel chg. (%)
IWV ( $kg.m^{-2}$ )	0.7	0.8	12.7	–	–	–
AR event (nb per year)	–	–	–	608	639	5.1
Precipitation ( $Gt.y^{-1}$ )	2981	3259	9.3	381	461	20.8
Rain ( $Gt.y^{-1}$ )	14	27	95.1	3.6	6.4	76.0
Snow ( $Gt.y^{-1}$ )	2967	3232	8.9	377	453	20.3
Melt ( $Gt.y^{-1}$ )	1074	1347	25.4	34	43	26.7

**Table 1.** AR statistics and SMB components, averaged over Antarctica: Historical and future periods, and relative changes for the complete climatology and AR-impacts only.

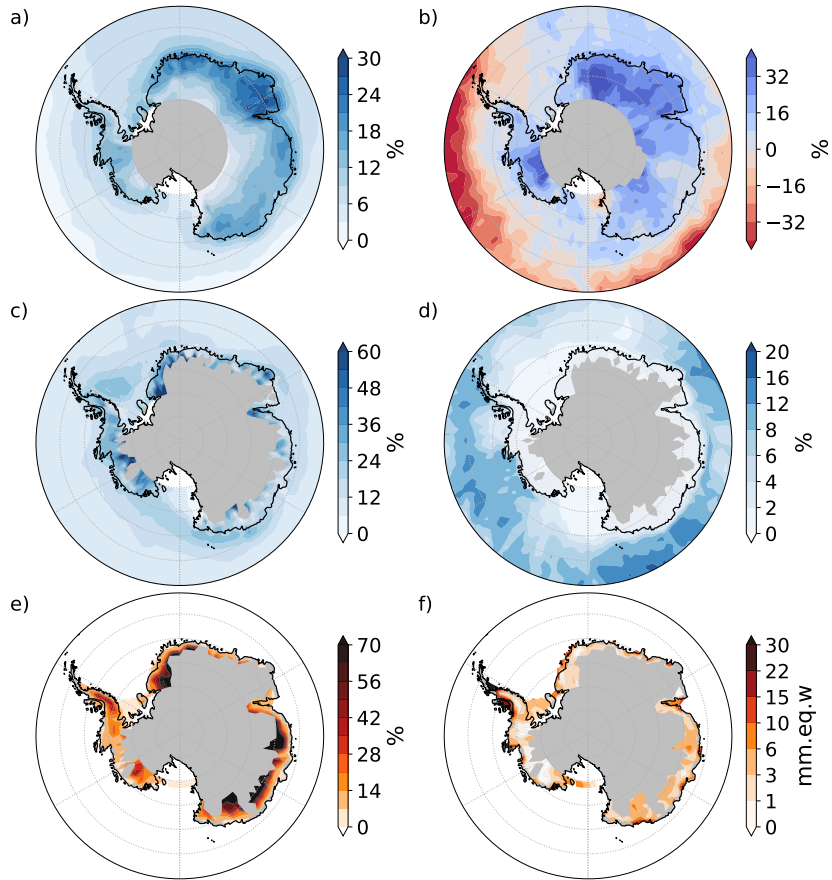


**Figure 4.** Left : contribution of ARs to the Antarctic SMB in the future period, shown as percentage of each total SMB component. Right: difference of the SMB components due to ARs between the future and historical periods. **a,b)** snowfall (future change due to ARs shown as relative difference), **c,d)** rainfall, and **e,f)** surface melt.

## 4 Discussion and Conclusion

The quantification of ARs in the future depends very much on the way in which they are detected, and in our case on the detection threshold used. A historical threshold based on current climatology detects a large increase in strong water vapor transport events in the future. But are all these events ARs? The increase in atmospheric humidity linked to rising temperatures seems to artificially increase the number of ARs detected by the algorithm (the increase in water transport is due to larger water amounts, not to mass fluxes), and therefore to induce biases when studying the occurrence and impacts of ARs defined as atmospheric dynamics features. This is confirmed by the use of a variable adaptive threshold. Taking into account the rise in background water vapor, the overall frequency of ARs detected in the polar zone remains constant over the entire 21st century (+1%), so an AR detected in the future will always be an extreme event relative to its contemporary climatic conditions.

Even with the use of the adaptive threshold, the frequency of ARs, their intensity, and their impacts over Antarctica appears to vary significantly in the future. While the overall increase in the number of AR event is small, the AR frequency over Antarctica and the number of AR events reaching the continent increase by +5%, following a spatial wave-number 3 pattern related to the mean circulation changes (mean poleward wind and storm tracks). This spatial pattern change is reflected in changes of AR-related precipitation. The intensity (maximum vIVT) of AR events increases in line with the Clausius-Clapeyron relation, leading to a shift of the intensity distribution towards higher values and a large increase in the probability of extreme events.

This increase in AR intensity naturally leads to larger impacts on the SMB. As shown in table 1, total precipitation over Antarctica will increase by +9.3% in the future (+95.1% for rain and +8.9% for snow), but the increase is larger for precipitation linked to ARs (+20%). This difference can be largely explained by the increase of the number of AR events as well as their mean duration.

The impact of ARs of surface melt (+26%) and rainfall (+76%) increases greatly, mostly caused by a more frequent crossing of the zero Celsius threshold. This increase is however not larger than their respective global values for Antarctica, even though the spatial pattern is different. The contribution of ARs to surface melt may decrease slightly at the coast, but becomes important in inland regions where neither melt nor rainfall occurred previously.

Therefore, while ARs are having an increasing impact on all components of the SMB, the dominant impact on the SMB of future ARs in our model is an increase of snowfall. However, this result is only true when considering averages over the whole continent. Rainfall and melting events are more concentrated, and will occur in some regions only in conjunction with ARs. Moreover, the GCM used cannot represent indirect effects such as the moistening of the firn and changes in snow albedo. The humidification of firn at depth also has an impact on melting processes (Harper et al., 2023) and on ice shelf destabilization (erosion and hydro-fracturing, (Pollard et al., 2015)) like at Amery ice shelf. Studies with more detailed models in key regions are thus needed to better quantify the total impacts on the overall mass balance, as well as other potential impacts, for example on ecosystems such as penguin colonies (Ganendran et al., 2016).

## 5 Open Research

CMIP6-IPSL data are available through the IPSL Computing and Data Center ES-PRI (Boucher et al., 2018, 2019). Catalogue of AR detection can be found at <https://doi.org/10.5281/zenodo.10848882>. Software in python and bash can be found at [https://github.com/lbarthelem/AR\\_antarctica](https://github.com/lbarthelem/AR_antarctica).

## Acknowledgments

This article is part of the ANR ARCA (Atmospheric River Climatology in Antarctica; grant number ANR-20-CE01-0013: <https://anr.fr/Project-ANR-20-CE01-0013>) funded by the French National Research Agency. All analyses were made with python (libraries numpy, pandas, scipy, sklearn, math, matplotlib, cartopy, seaborn, netCDF4, xarray), the developers of which are thanked. Calculations were performed using IPSL resources from IPSL Computing and Data Center ESPRI. We would also like to thank the Quantarctica project (Matsuoka et al., 2018) for the availability of mapping data.

## References

- Baek, S. H., & Lora, J. M. (2021, October). Counterbalancing influences of aerosols and greenhouse gases on atmospheric rivers. *Nature Climate Change*, 1–8. Retrieved 2021-10-12, from <http://www-nature-com/articles/s41558-021-01166-8> (Bandiera.abtest: a Cg\_type: Nature Research Journals Primary\_atype: Research Publisher: Nature Publishing Group Subject\_term: Atmospheric dynamics;Climate change;Hydrology Subject\_term.id: atmospheric-dynamics;climate-change;hydrology) doi: 10.1038/s41558-021-01166-8
- Boucher, O., Denvil, S., Levassasseur, G., Cozic, A., Caubel, A., Foujols, M.-A., ... Cheruy, F. (2018). *IPSL IPSL-CM6A-LR model output prepared for CMIP6 CMIP historical*. Earth System Grid Federation. Retrieved from <https://doi.org/10.22033/ESGF/CMIP6.5195> doi: 10.22033/ESGF/CMIP6.5195
- Boucher, O., Denvil, S., Levassasseur, G., Cozic, A., Caubel, A., Foujols, M.-A., ... Lurton, T. (2019). *Ipsl ipsl-cm6a-lr model output prepared for cmip6 scenar-iomip*. Earth System Grid Federation. Retrieved from <https://doi.org/10.22033/ESGF/CMIP6.1532> doi: 10.22033/ESGF/CMIP6.1532
- Bozkurt, D., Rondanelli, R., Marín, J. C., & Garreaud, R. (2018). Foehn Event Triggered by an Atmospheric River Underlies Record-Setting Temperature Along Continental Antarctica. *Journal of Geophysical Research: Atmospheres*, 123(8), 3871–3892. Retrieved 2024-02-29, from <https://onlinelibrary.wiley.com/doi/abs/10.1002/2017JD027796> (.eprint: <https://onlinelibrary.wiley.com/doi/pdf/10.1002/2017JD027796>) doi: 10.1002/2017JD027796
- Datta, R. T., Tedesco, M., Fettweis, X., Agosta, C., Lhermitte, S., Lenaerts, J. T. M., & Wever, N. (2019). The effect of foehn-induced surface melt on firn evolution over the northeast antarctic peninsula. *Geophysical Research Letters*, 46, 3822–3831. doi: 10.1029/2018GL080845
- Fretwell, P., Pritchard, H. D., Vaughan, D. G., Bamber, J. L., Barrand, N. E., Bell, R., ... Zirizzotti, A. (2013, February). Bedmap2: improved ice bed, surface and thickness datasets for Antarctica. *The Cryosphere*, 7(1), 375–393. Retrieved 2023-05-09, from <https://tc.copernicus.org/articles/7/375/2013/> (Publisher: Copernicus GmbH) doi: 10.5194/tc-7-375-2013
- Ganendran, L. B., Sidhu, L. A., Catchpole, E. A., Chambers, L. E., & Dann, P. (2016, August). Effects of ambient air temperature, humidity and rainfall on annual survival of adult little penguins *Eudyptula minor* in southeastern Australia. *International Journal of Biometeorology*, 60(8), 1237–1245. Retrieved 2024-01-23, from <https://doi.org/10.1007/s00484-015-1119-2> doi: 10.1007/s00484-015-1119-2
- Gorodetskaya, I. V., Tsukernik, M., Claes, K., Ralph, M. F., Neff, W. D., & Lipzig, N. P. M. V. (2014). The role of atmospheric rivers in anomalous snow accumulation in East Antarctica. *Geophysical Research Letters*, 41(17), 6199–6206. Retrieved 2021-06-05, from <https://agupubs.onlinelibrary.wiley.com/doi/abs/10.1002/2014GL060881> (.eprint: <https://agupubs.onlinelibrary.wiley.com/doi/pdf/10.1002/2014GL060881>) doi: <https://doi.org/10.1002/2014GL060881>

- 348 Harper, J., Saito, J., & Humphrey, N. (2023). Cold Season Rain Event Has Im-  
 349 pact on Greenland’s Firn Layer Comparable to Entire Summer Melt Season.  
 350 *Geophysical Research Letters*, *50*(14), e2023GL103654. Retrieved 2023-10-13,  
 351 from <https://onlinelibrary.wiley.com/doi/abs/10.1029/2023GL103654>  
 352 (\_eprint: <https://onlinelibrary.wiley.com/doi/pdf/10.1029/2023GL103654>) doi:  
 353 10.1029/2023GL103654
- 354 Jakobs, C. L., Reijmer, C. H., Kuipers Munneke, P., König-Langlo, G., & van den  
 355 Broeke, M. R. (2019). Quantifying the snowmelt–albedo feedback at neu-  
 356 mayer station, east antarctica. *The Cryosphere*, *13*(5), 1473–1485. doi:  
 357 10.5194/tc-13-1473-2019
- 358 Kuipers Munneke, P., Luckman, A. J., Bevan, S. L., Smeets, C. J. P. P., Gilbert, E.,  
 359 van den Broeke, M. R., ... Kulesa, B. (2018). Intense winter surface melt  
 360 on an antarctic ice shelf. *Geophysical Research Letters*, *45*, 7615–7623. doi:  
 361 10.1029/2018GL077899
- 362 Matsuoka, K., Skoglund, A., Roth, G., de Pomereu, J., Griffiths, H., Headland,  
 363 R., & Melvær, Y. (2018). *Quantarctica*. Norwegian Polar Institute. Re-  
 364 trieved from <https://doi.org/10.21334/npolar.2018.8516e961> doi:  
 365 10.21334/npolar.2018.8516e961
- 366 Nash, D., Waliser, D., Guan, B., Ye, H., & Ralph, F. M. (2018). The Role of  
 367 Atmospheric Rivers in Extratropical and Polar Hydroclimate. *Journal of Geo-*  
 368 *physical Research: Atmospheres*, *123*(13), 6804–6821. Retrieved 2023-11-20,  
 369 from <https://onlinelibrary.wiley.com/doi/abs/10.1029/2017JD028130>  
 370 (\_eprint: <https://onlinelibrary.wiley.com/doi/pdf/10.1029/2017JD028130>) doi:  
 371 10.1029/2017JD028130
- 372 Neff, W., Compo, G. P., Martin Ralph, F., & Shupe, M. D. (2014). Con-  
 373 tinental heat anomalies and the extreme melting of the Greenland ice  
 374 surface in 2012 and 1889. *Journal of Geophysical Research: Atmo-*  
 375 *spheres*, *119*(11), 6520–6536. Retrieved 2024-02-29, from [https://](https://onlinelibrary.wiley.com/doi/abs/10.1002/2014JD021470)  
 376 [onlinelibrary.wiley.com/doi/abs/10.1002/2014JD021470](https://onlinelibrary.wiley.com/doi/abs/10.1002/2014JD021470) (\_eprint:  
 377 <https://onlinelibrary.wiley.com/doi/pdf/10.1002/2014JD021470>) doi:  
 378 10.1002/2014JD021470
- 379 Payne, A. E., Demory, M.-E., Leung, L. R., Ramos, A. M., Shields, C. A., Rutz,  
 380 J. J., ... Ralph, F. M. (2020, March). Responses and impacts of atmo-  
 381 spheric rivers to climate change. *Nature Reviews Earth & Environment*, *1*(3),  
 382 143–157. Retrieved 2022-02-15, from [https://www.nature.com/articles/](https://www.nature.com/articles/s43017-020-0030-5)  
 383 [s43017-020-0030-5](https://www.nature.com/articles/s43017-020-0030-5) (Number: 3 Publisher: Nature Publishing Group) doi:  
 384 10.1038/s43017-020-0030-5
- 385 Pollard, D., DeConto, R. M., & Alley, R. B. (2015, February). Potential Antarc-  
 386 tic Ice Sheet retreat driven by hydrofracturing and ice cliff failure. *Earth and*  
 387 *Planetary Science Letters*, *412*, 112–121. Retrieved 2023-10-13, from [https://](https://www.sciencedirect.com/science/article/pii/S0012821X14007961)  
 388 [www.sciencedirect.com/science/article/pii/S0012821X14007961](https://www.sciencedirect.com/science/article/pii/S0012821X14007961) doi: 10  
 389 .1016/j.epsl.2014.12.035
- 390 Ralph, F. M., Rutz, J. J., Cordeira, J. M., Dettinger, M., Anderson, M., Reynolds,  
 391 D., ... Smallcomb, C. (2019, February). A Scale to Characterize the  
 392 Strength and Impacts of Atmospheric Rivers. *Bulletin of the American Me-*  
 393 *teorological Society*, *100*(2), 269–289. Retrieved 2021-11-23, from [https://](https://journals.ametsoc.org/view/journals/bams/100/2/bams-d-18-0023.1.xml)  
 394 [journals.ametsoc.org/view/journals/bams/100/2/bams-d-18-0023.1.xml](https://journals.ametsoc.org/view/journals/bams/100/2/bams-d-18-0023.1.xml)  
 395 (Publisher: American Meteorological Society Section: Bulletin of the American  
 396 Meteorological Society) doi: 10.1175/BAMS-D-18-0023.1
- 397 Shields, C. A., Payne, A. E., Shearer, E. J., Wehner, M. F., O’Brien, T. A.,  
 398 Rutz, J. J., ... Zarzycki, C. (2023). Future Atmospheric Rivers  
 399 and Impacts on Precipitation: Overview of the ARTMIP Tier 2 High-  
 400 Resolution Global Warming Experiment. *Geophysical Research Let-*  
 401 *ters*, *50*(6), e2022GL102091. Retrieved 2023-03-30, from [https://](https://onlinelibrary.wiley.com/doi/abs/10.1029/2022GL102091)  
 402 [onlinelibrary.wiley.com/doi/abs/10.1029/2022GL102091](https://onlinelibrary.wiley.com/doi/abs/10.1029/2022GL102091) (\_eprint:

- 403 <https://agupubs.onlinelibrary.wiley.com/doi/pdf/10.1029/2022GL102091> doi:  
404 10.1029/2022GL102091
- 405 Turner, J., Phillips, T., Thamban, M., Rahaman, W., Marshall, G. J., Wille,  
406 J. D., ... Lachlan-Cope, T. (2019). The Dominant Role of Extreme Pre-  
407 cipitation Events in Antarctic Snowfall Variability. *Geophysical Research*  
408 *Letters*, 46(6), 3502–3511. Retrieved 2021-02-10, from [https://agupubs](https://agupubs.onlinelibrary.wiley.com/doi/abs/10.1029/2018GL081517)  
409 [.onlinelibrary.wiley.com/doi/abs/10.1029/2018GL081517](https://agupubs.onlinelibrary.wiley.com/doi/abs/10.1029/2018GL081517) (eprint:  
410 <https://agupubs.onlinelibrary.wiley.com/doi/pdf/10.1029/2018GL081517>) doi:  
411 <https://doi.org/10.1029/2018GL081517>
- 412 Vignon, E., Hourdin, F., Genthon, C., Van de Wiel, B. J. H., Gallée, H.,  
413 Madeleine, J.-B., & Beaumet, J. (2018). Modeling the Dynam-  
414 ics of the Atmospheric Boundary Layer Over the Antarctic Plateau  
415 With a General Circulation Model. *Journal of Advances in Modeling*  
416 *Earth Systems*, 10(1), 98–125. Retrieved 2024-01-12, from [https://](https://onlinelibrary.wiley.com/doi/abs/10.1002/2017MS001184)  
417 [onlinelibrary.wiley.com/doi/abs/10.1002/2017MS001184](https://onlinelibrary.wiley.com/doi/abs/10.1002/2017MS001184) (eprint:  
418 <https://onlinelibrary.wiley.com/doi/pdf/10.1002/2017MS001184>) doi:  
419 10.1002/2017MS001184
- 420 Vignon, E., Roussel, M.-L., Gorodetskaya, I., Genthon, C., & Berne, A. (2021).  
421 Present and future of rainfall in antarctica. *Geophysical Research Letters*,  
422 48(8), e2020GL092281.
- 423 Wessem, J. M. V., Reijmer, C. H., Morlighem, M., Mouginot, J., Rignot, E., Medley,  
424 B., ... Meijgaard, E. V. (2014). Improved representation of east antarctic  
425 surface mass balance in a regional atmospheric climate model. *Journal of*  
426 *Glaciology*, 60, 761–770. doi: 10.3189/2014JoG14J051
- 427 Wille, J. D., Favier, V., Dufour, A., Gorodetskaya, I. V., Turner, J., Agosta,  
428 C., & Codron, F. (2019, October). West Antarctic surface melt trig-  
429 gered by atmospheric rivers. *Nature Geoscience*. Retrieved 2019-10-  
430 29, from <http://www.nature.com/articles/s41561-019-0460-1> doi:  
431 10.1038/s41561-019-0460-1
- 432 Wille, J. D., Favier, V., Gorodetskaya, I. V., Agosta, C., Kittel, C., Beeman,  
433 J. C., ... Codron, F. (2021). Antarctic Atmospheric River Climatol-  
434 ogy and Precipitation Impacts. *Journal of Geophysical Research: Atmo-*  
435 *spheres*, 126(8), e2020JD033788. Retrieved 2021-04-14, from [http://](http://agupubs.onlinelibrary.wiley.com/doi/abs/10.1029/2020JD033788)  
436 [agupubs.onlinelibrary.wiley.com/doi/abs/10.1029/2020JD033788](http://agupubs.onlinelibrary.wiley.com/doi/abs/10.1029/2020JD033788)  
437 (eprint: <https://onlinelibrary.wiley.com/doi/pdf/10.1029/2020JD033788>)  
438 doi: <https://doi.org/10.1029/2020JD033788>
- 439 Zhang, L., Zhao, Y., Cheng, T. F., & Lu, M. (2024). Future Changes in Global  
440 Atmospheric Rivers Projected by CMIP6 Models. *Journal of Geophysi-*  
441 *cal Research: Atmospheres*, 129(3), e2023JD039359. Retrieved 2024-02-05,  
442 from <https://onlinelibrary.wiley.com/doi/abs/10.1029/2023JD039359>  
443 (eprint: <https://onlinelibrary.wiley.com/doi/pdf/10.1029/2023JD039359>) doi:  
444 10.1029/2023JD039359

Figure 1.

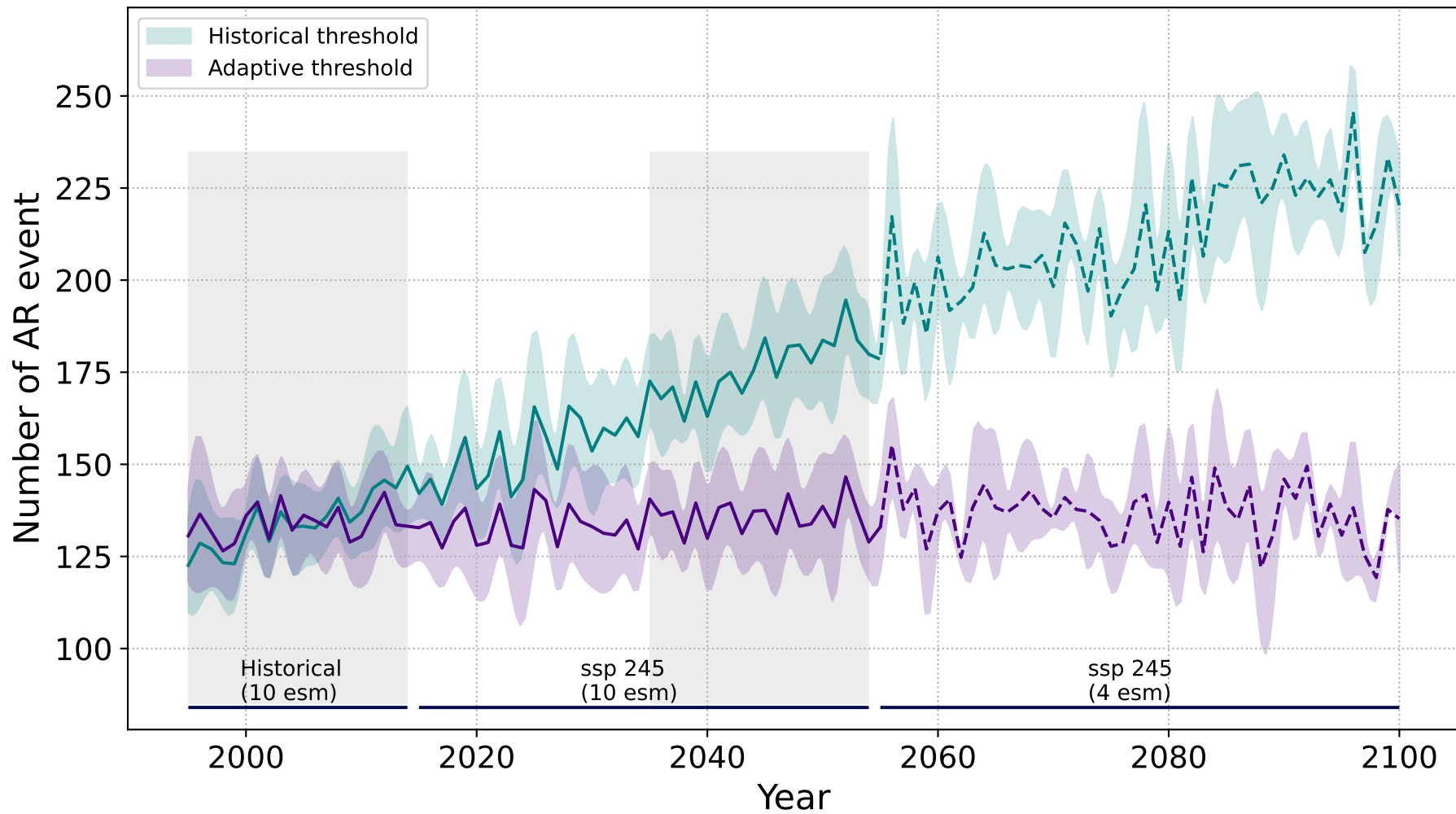


Figure 2.

a)

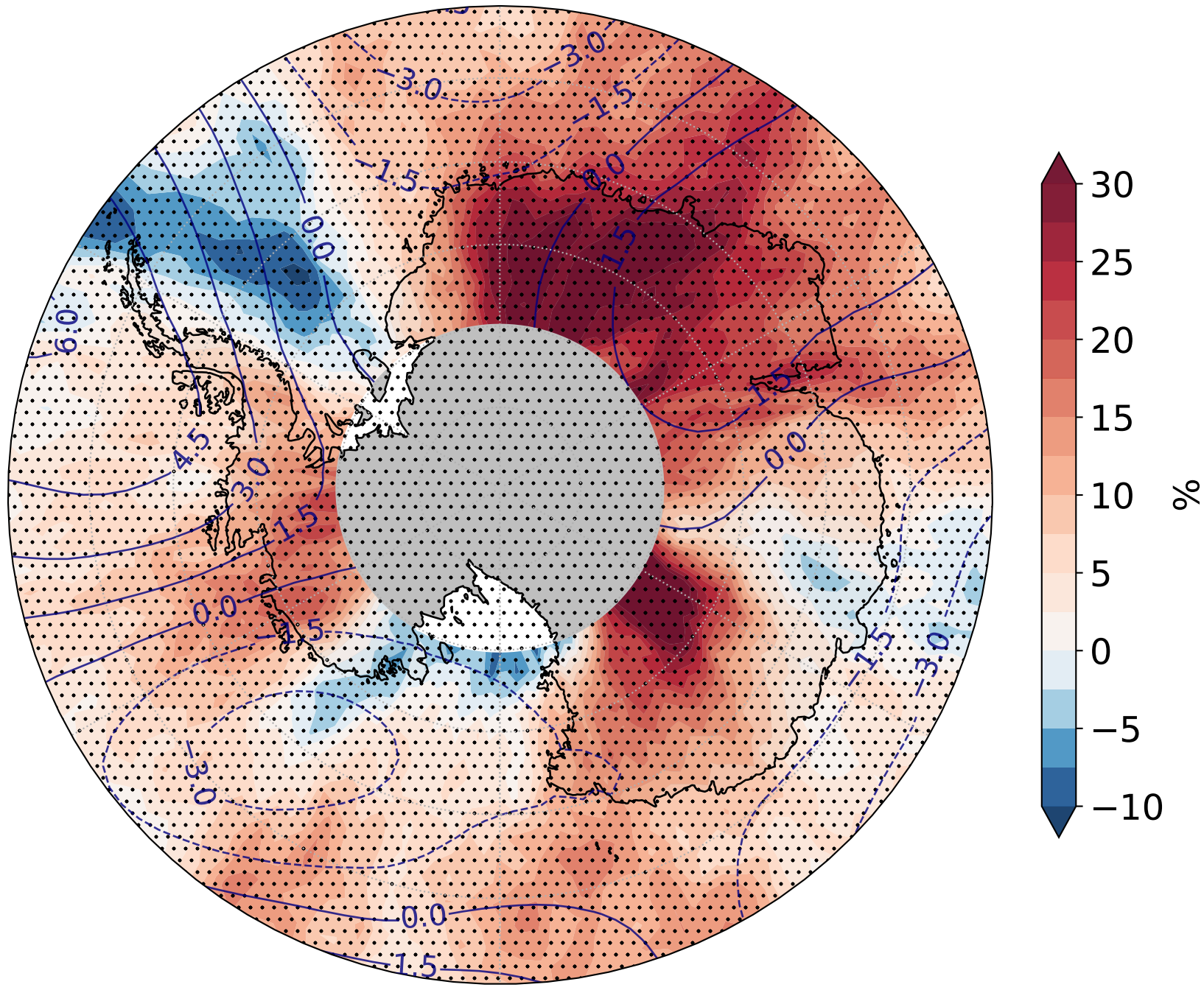


Figure 3.

Historical threshold

Adaptive threshold

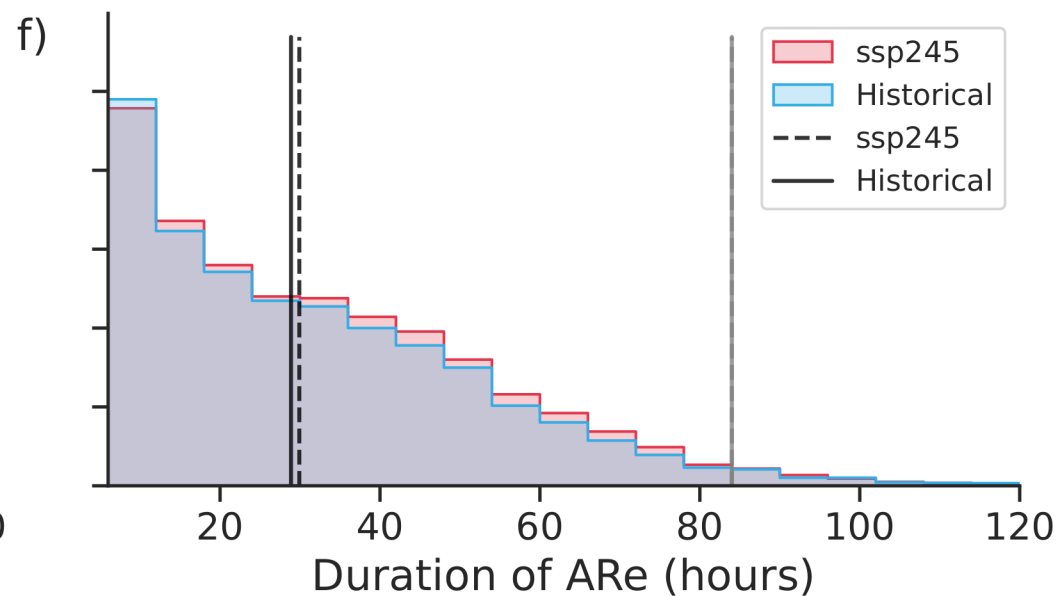
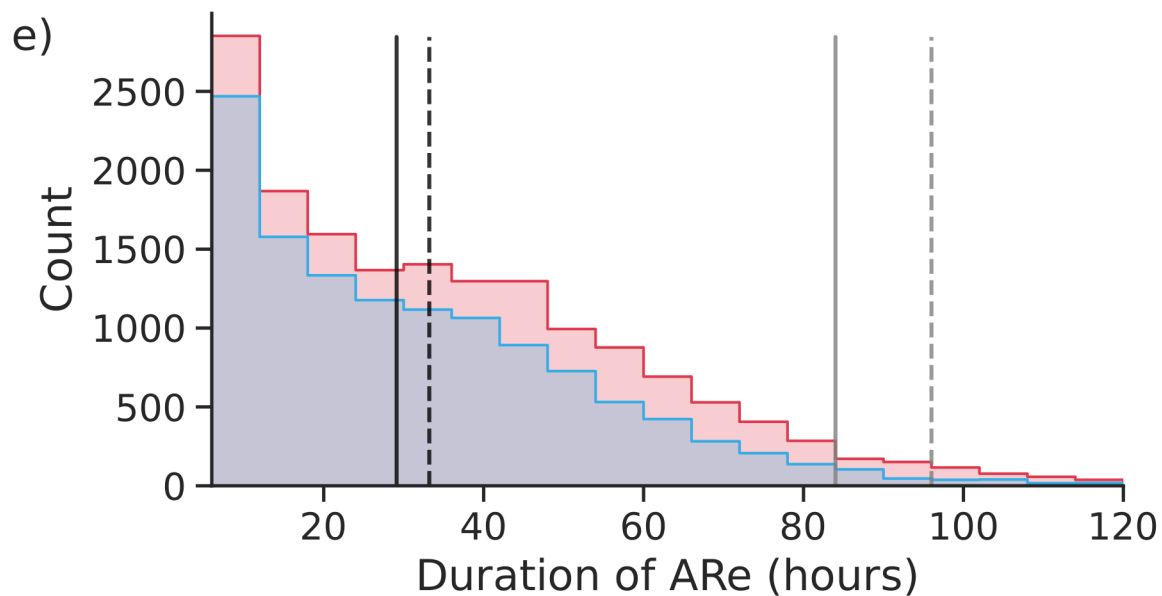
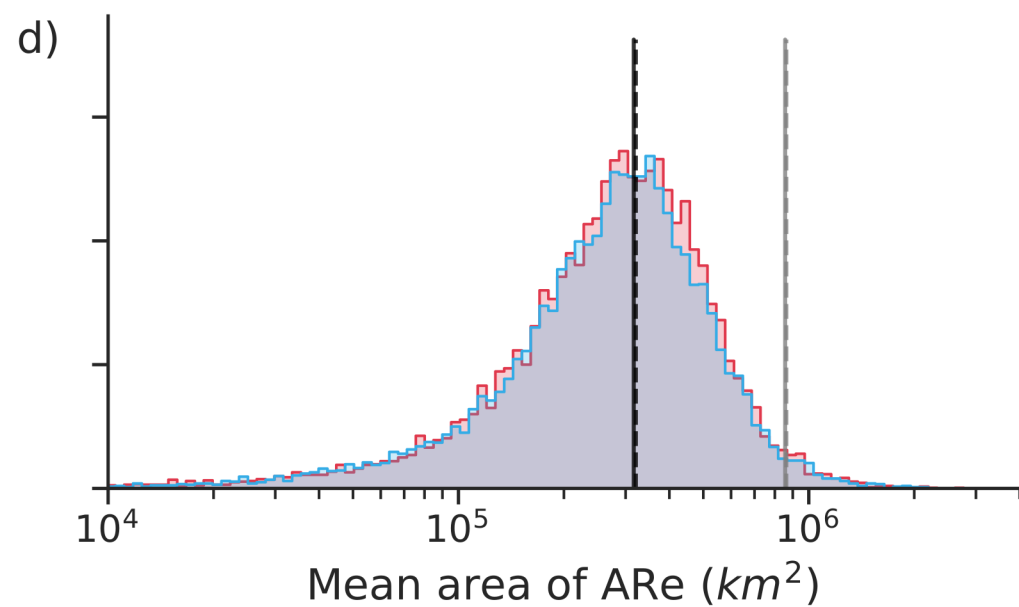
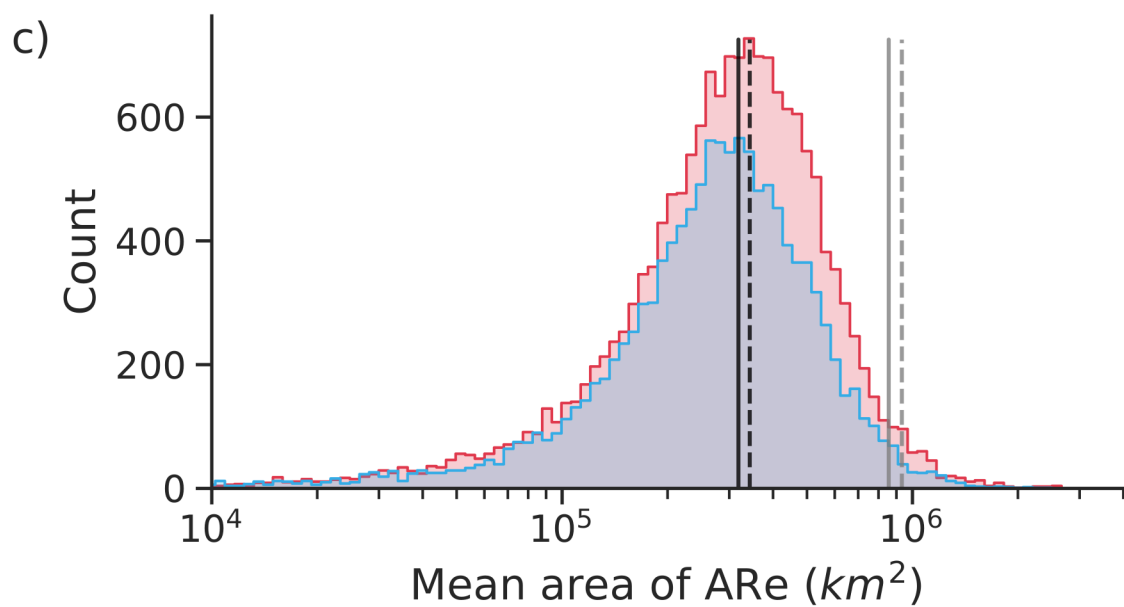
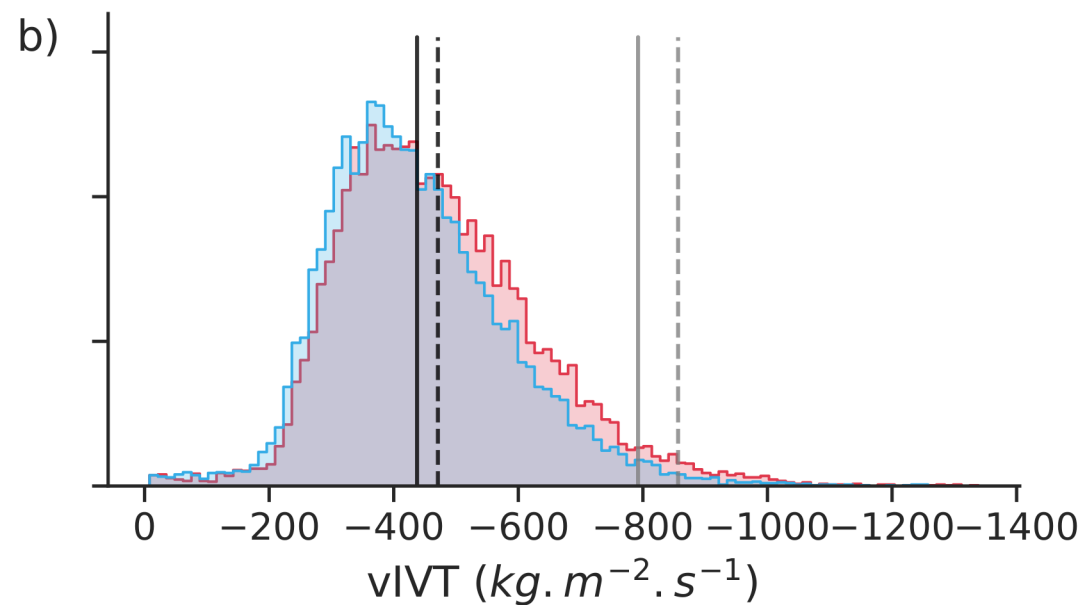
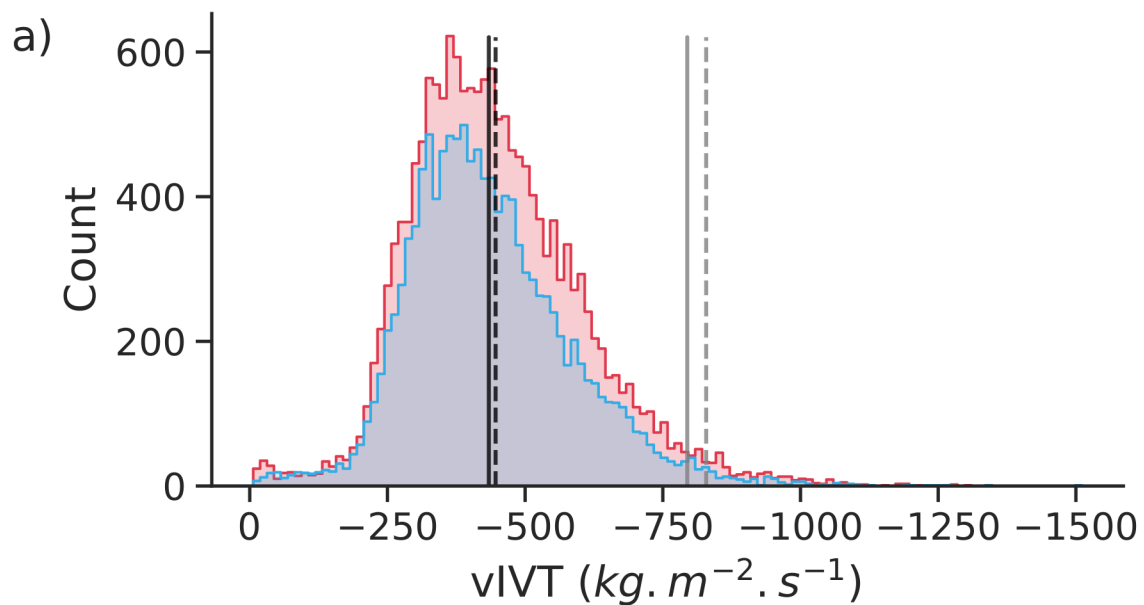


Figure 4.

